Figure 11. The predicted-to-observed SF_6 concentration ratio values from the advection-diffusion model.

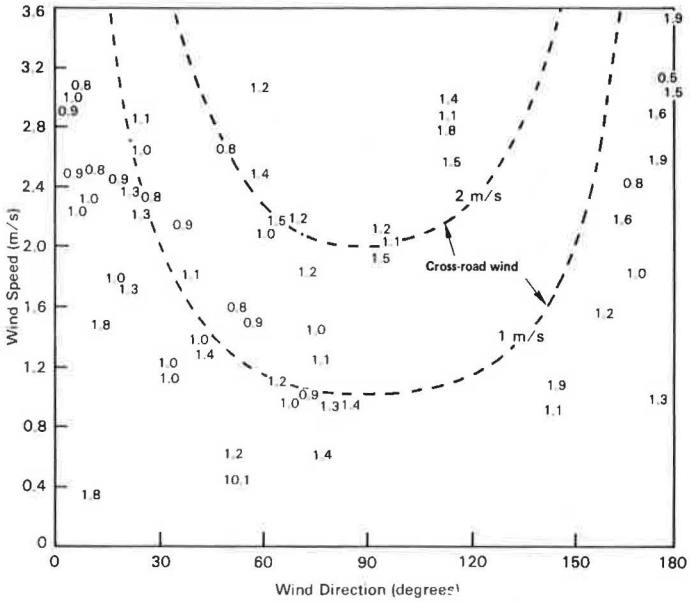

of Atmospheric Turbulence. Wiley, New York, 1964.
9. D. P. Chock. General Motors Sulfate Dispersion Experiment—An Overview of the Wind, Temperature and Concentration Fields. Atmospheric Environment, Vol. 11, 1977, pp. 553-559.
10. D. B. Turner. Workbook of Atmospheric Dispersion Estimates. U.S. Public Health Service, National Center for Air Pollution Control, Cincinnati, Publ. 999-AP-26, 1968.
11. D. P. Chock. General Motors Sulfate Dispersion Experiment: Assessment of the EPA HIWAY Model. Journal of the Air Pollution Control Association, Vol. 27, 1977, pp. 39-45.
12. D. P. Chock. A Simple Line-Source Model for Dispersion Near Roadways. General Motors Research Laboratories, Warren, MI, GMR-2407, May 29, 1977.
13. D. P. Chock. An Advection-Diffusion Model for Pollutant Dispersion Near Roadways. General Motors Research Laboratories, Warren, MI, GMR-2590, Nov. 1977.

Atmospheric and Wind Tunnel Studies of Air Pollution Dispersion Near Highways

Walter F. Dabberdt, Atmospheric Sciences Laboratory, Stanford Research Institute International, Menlo Park, California
Howard A. Jongedyk, Office of Research, Federal Highway Administration

Atmospheric and wind tunnel studies of gaseous dispersion near roadways have identified new concepts regarding the influence of roadway traffic and stimulated the development of a versatile yet simple simulation model, ROADMAP. Influences of site geometry and roadway configurations were observed and quantified. Two effects found to be particularly significant to microscale dispersion were (a) thermal turbulence and buoyancy caused by vehicular waste heat and (b) mechanical turbulence from highway traffic. ROADMAP simulates two-dimensional gaseous dispersion patterns for various roadway configurations including grade-level, vertical, and slant-wall cut, fill, and viaduct sections. Development of the model is first detailed for a uniform, grade-level freeway. Dispersion patterns were obtained up to heights of 14 m and to downwind distances of 100 m by a sampling array that measured meteorological conditions and concentrations of carbon monoxide and two artificial tracer gases released in the traffic. Comparison of equivalent field and wind-tunnel tests for grade-level roads shows good agreement except for acute wind-roadway angles. ROADMAP's capability for varied site geometries was evaluated by analyzing field and wind tunnel tests for 20 roadway configurations. Comparisons of ROADMAP to independent carbon monoxide data (i.e., data not used in developing the model) from the grade-level field tests resulted in high values of the linear correlation coefficient: 0.91 for neutral stability, 0.67 for stable atmospheric conditions, and 0.80 for unstable conditions. Values for the cut and elevated-section tests in the wind tunnel ranged from 0.69 to 0.93.

The air pollutants entrained and subsequently dispersed by highway traffic depend on the meteorological characteristics generally prevailing in the specified loca-

tion for a given time, the local terrain and road site, and the roadway vehicles. The nature and magnitude of the the dispersion are affected by the general speed and direction of the wind passing over the roadway as well as by the induced air motions and turbulence generated by the highway and traffic. A part of the fluctuations and turbulence comes from vehicle presence and operations that produce heat as well as aerodynamic disturbances, such as wakes. The turbulence from highway traffic is a complexity of wall, free, and convective types.

Estimates of air pollutant dispersion near roadways have usually not given adequate consideration to the fluid mechanics involved. Accurate estimates are necessary to gauge receptor impacts and plan remedial measures. A thorough three-dimensional analytical model, however, is still unverifiable and could be unwieldy or impractical at this time. Nonetheless, to increase the conceptual understanding of the air flows and quality on and near roadways, the Federal Highway Administration (FHWA) has had an extensive study conducted by Stanford Research Institute International.

A new model, the roadway atmospheric dispersion model for air pollution (ROADMAP), utilizes the experimental work of this study and considers highway geometry, vehicle waste heat, and turbulence. The focus is on relatively simple, definable, and common highway traffic situations. Included in ROADMAP are coordinated tasks in fluid dynamic evaluations, explorations of other pertinent measurements, analytical modeling, scale model wind tunnel tests, extensively measured highway field location, descriptive modeling, and trial applications.

EXPERIMENTAL PROGRAM

Aerometric measurements were made near a wide range of roadway configurations to investigate the dispersion process as it relates to site geometry, traffic conditions, and meteorology. Atmospheric field tests were conducted under various atmospheric and traffic conditions at grade-level, vertical-wall cut, and viaduct sections. A broader range of site geometries was considered during the more than 300 wind tunnel tests: 17 configurations were studied under varying traffic and wind conditions (stability, however, was always neutral). Included were at-grade level sections of varied smooth and rough terrain, vertical- and slant-wall cut, airtight structure, fill, viaduct, and hillside sections.

Figure 1. Photograph of grade-level highway test site.

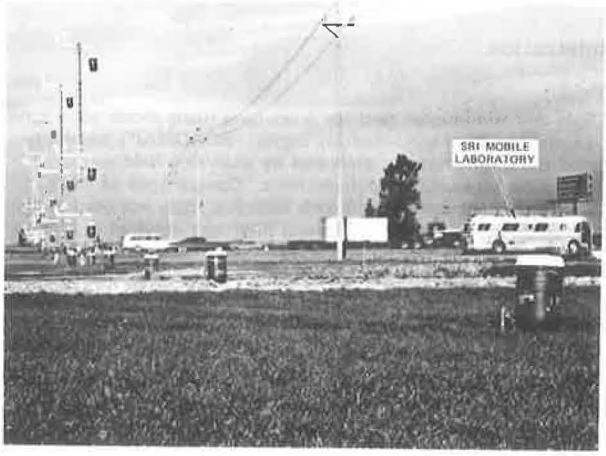

Field Sites

Traffic and meteorological effects were investigated at a flat, grade-level location for wind-tunnel test comparisons and to avoid the aerodynamic complexities of the other, more intricate site configurations. Results of the tests at the highway-cut section and viaduct section provided useful concepts but, because of limited use in model development, discussion here focuses on the at-grade site. Measurements for that site were made in 1975 on US-101 (Bayshore Freeway) in Santa Clara, California, 80 km southeast of San Francisco. The road is a major intrastate freeway of three lanes of traffic in each direction; the roadway is oriented nearly east-west at the test site. The traffic flow is heavy [around 110 000 average daily traffic (ADT)] and varies markedly throughout the day, both in speed and in volume by direction.

The median strip is sufficiently wide to permit installation of towers (five were used) for meteorological and air sampling purposes. A comprehensive micro-sampling network monitored wind, temperature, air quality, and traffic. Figures 1 and 2 illustrate the location and orientation of the aerometric instrumentation. Ambient meteorological data were measured at four heights (2.0, 3.8, 7.5, and 14.2 m) on the five towers. Wind and turbulence measurements were made on all five towers, but precision temperature profiles were only measured on the two towers adjacent to the roadway edges. All 50 meteorological data inputs were sampled, digitized, and recorded on magnetic tape every 2.5 s. Hourly and 15-min summaries of primary and derived parameters were prepared. Comprehensive traffic information about speed and axle number for each vehicle, segregated on a lane-by-lane basis, was recorded throughout the study period. Summaries were also tabulated every 15 min for each of the 45 h encompassed by the study.

Sequential multiple-bag samplers were programmed to obtain hourly air samples of 4 L at each of 35 locations (see Figure 1); 20 samplers were located at the ground surface out to 100 m from the roadway edges and 15 were placed on the towers. The air samples were analyzed to determine ambient concentrations of carbon monoxide (CO), total hydrocarbons (THC), and methane (CH_4), in addition to concentrations of two tracer gases [sulfur hexafluoride (SF_6) and fluorotribromomethane ($CFlBr_3$)] released on the highway. Two vans were equipped to release each of the two tracer gases. They were driven continuously in the traffic stream, always in the middle lane at general speed, but not exceeding 90 km/h (55 mph). The drivers released SF_6 in the west direction and $CFlBr_3$ in the east direction.

Wind Tunnel Studies

The principal component of the highway model used in the Calspan wind tunnel was a moving roadway. Its function is to distribute the exhausts from model vehicles in analogy to the full-scale situations. The model vehicles were attached to two moving belts; for most tests two lanes of traffic were attached to each belt. The belts could be driven in the same or in opposite directions. Beneath the belts a plenum chamber supplied a He-N gas mixture, which was vented to the atmosphere through exhaust ports on each vehicle. In turn, the entire roadway model was constructed to fit into the 2.2-m diameter turntable in the floor of the wind tunnel; by rotating the turntable, the angle between the wind vector and roadway axis was easily varied. The thin roadway-plenum chamber construction enabled the model

to be elevated to simulate a viaduct, fill, or hillside section; by lowering the model roadway, cut sections were also simulated. The model cars and trucks were mounted on belts of two different spacing configurations: high density of an average spacing of two car lengths, and a low-density spacing of four car lengths.

Capillary tubes were used at 20 locations to sample the air near the roadway for pollutant concentrations. The He concentration in each sample was then determined with a He-leak detector, modified to provide a direct reading of the concentration.

TURBULENCE DATA

Values of the total (i.e., three-component) intensity of turbulence (TTI) from the US-101, grade-level roadway experiment were compared at each of several heights among near-upwind, median, and near-downwind sensor locations. As used here, TTI is defined as

$$TTI \equiv \left[\overline{(u')^2 + (v')^2 + (w')^2}\right]^{1/2} \quad (1)$$

where

u = the longitudinal wind component,
v = the lateral wind component, and
w = the vertical wind component.

The prime notation denotes the departure from the period average; the overbar denotes the period average of the function. The south-to-north turbulence gradient [ΔTTI ≡ TTI (north) - TTI (south)] between sensors 10.5 m from either edge of the roadway ranged from +0.50 to -0.50 m/s at the 2.0-, 3.8-, and 7.5-m levels with southerly and northerly winds, respectively; at 14.2 m, the range was ±0.35 m/s. When ΔTTI is normalized by dividing by the upwind turbulence intensity at corresponding heights, the range of maximum normalized gradients has a similar height dependence: ±1.5 at 2 m; +2.0 to -1.0 at 7.5 m; and ±0.75 at 14.2 m. Similar comparisons made among the upwind (near-roadway) values and the turbulence data measured in the roadway median show this median-upwind gradient to range up to -1.10 m/s at 2 m, to -1.20 m/s at 3.8 m, and to -0.60 m/s at 7.5 m (see Figure 3).

The turbulence data were also grouped into six wind-direction categories and correlated with various independent traffic and meteorological variables; 13 independent variables were defined using the following basic parameters:

1. Upwind turbulence intensity,
2. Upwind wind speed,
3. Cross-roadway wind speed component,
4. Cross-roadway temperature gradient,
5. Vehicle volume,
6. Vehicle speed, and
7. The computed vehicle drag-induced ambient flow.

The south-to-north turbulence gradient correlated consistently over the six wind-direction categories with only one parameter, the south-to-north temperature gradient. Even so, the average correlation coefficient of 0.55 (and 0.40 for normalized ΔTTI) is not particularly significant. The average correlation for winds ≥ 45° to the road increased to 0.68 for the normalized turbulence gradient and remained at 0.55 for the nonnormalized gradient. The upwind-median gradient of turbulence correlated consistently with only the upwind wind speed (u_{ref}). The average correlation coefficient for TTI and u_{ref} was 0.47 for all categories and only 0.32 for winds ≥ 45° to the road. The normalized TTI correlated with u_{ref} at 0.56 for all directions and at 0.51 for the more oblique directions.

TEMPERATURE DATA

Temperatures measured 10.5 m from either edge of the roadway at the grade-level site showed significant cross-roadway gradients [ΔT ≡ T(north) - T(south)]. At the 2-m level, south-to-north gradients ranged up to 2.5°C for southerly winds and up to -1.5° C for northerly winds. At 3.8 m, ΔT ranged from +1.5° to -0.75°C for northerly and southerly winds (Figure 4), respectively, and at 7.5 m the range was +0.75° to

Figure 2. Aerometric instrumentation layout at grade-level test site.

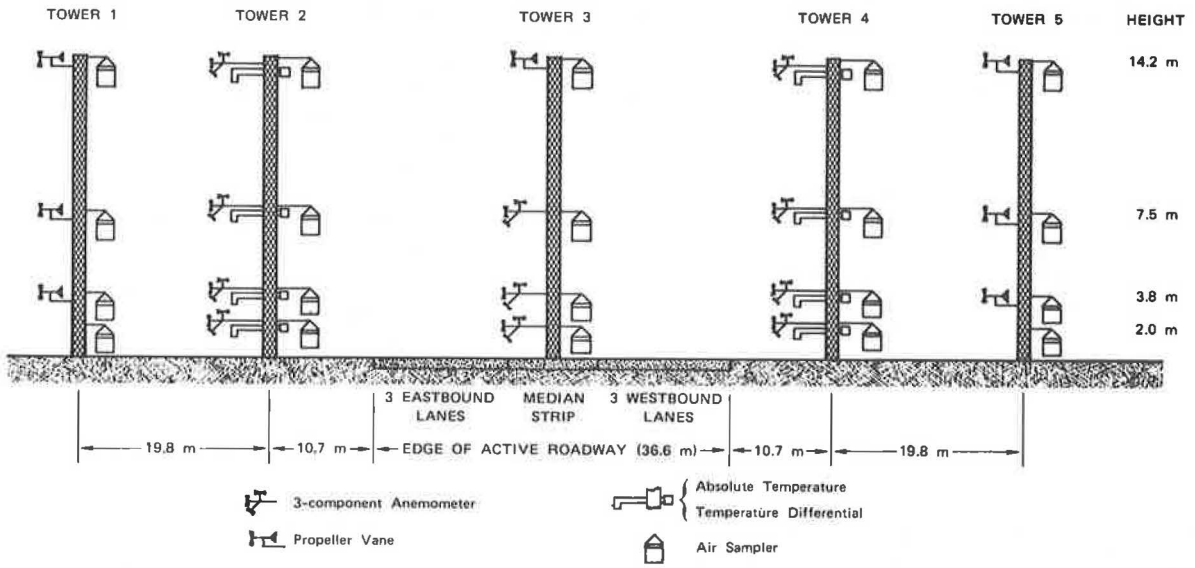

NOTE: Additional air samplers located at ground level on both sides of road beyond towers at 15.2 m intervals to 91.5 m from roadway edges.

Figure 3. Wind directional variation of the normal upwind-minus-median turbulence intensity.

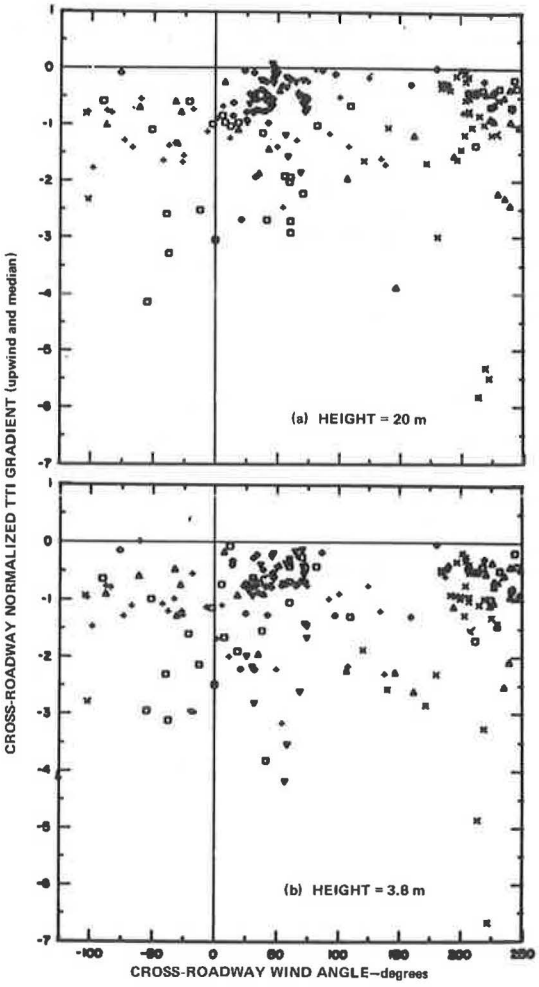

Figure 4. Variation of cross-roadway temperature gradient with wind direction.

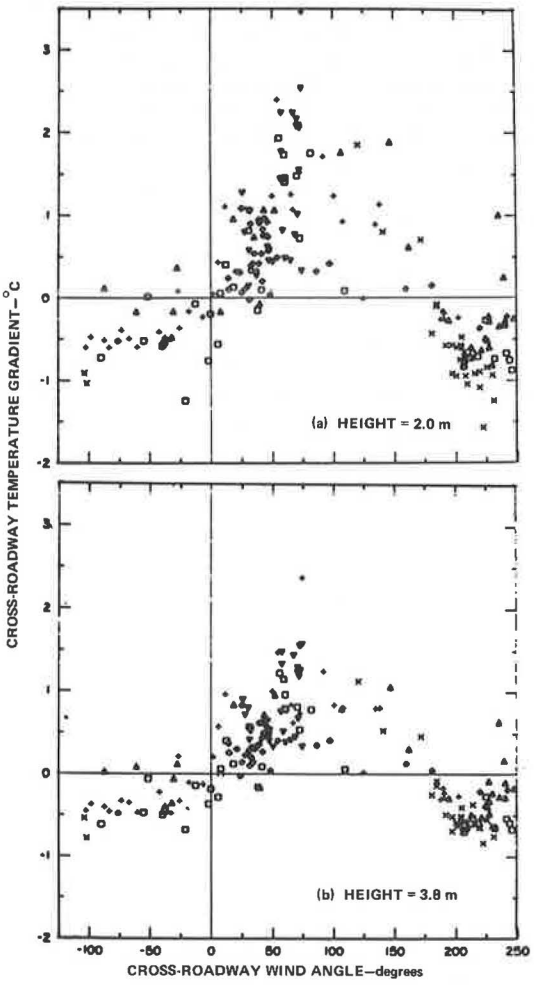

-0.4°C. The temperature gradient data were stratified into six 15° (arc) categories according to the absolute value of the angle between the wind vector and the roadway bearing. The ΔT data were then correlated within each of the six categories with each of six independent variables:

1. Upwind turbulence intensity,
2. Cross-roadway wind speed,
3. The product of 1 and 2,
4. Vehicle volume,
5. The product of vehicle volume and speed, and
6. The quotient of 5 and 3.

The only consistently significant linear correlation coefficient ($\bar{r}$ = 0.71) was with the cross-roadway wind speed (u_{road}). A scatter plot of ΔT versus u_{road} shows that at low wind speeds, T increases with increasing u_{road} values.

The near-roadway vertical temperature data are important for two reasons: (a) they provide an indication of the thermal stability of the air near the roadway and thus serve to describe the diffusion characteristics of the air into which vehicular pollutants are emitted; and (b) they serve as a tracer of vehicle pollutant emissions. Before the full utility of the temperature data can be assessed, it is necessary to understand the causes of the observed cross-roadway temperature gradients. Three processes are potential contributors: (a) vehicle waste heat emissions; (b) differences in the atmospheric sensible heat flux among the clay soil of upwind fetches and the concrete and asphalt surfaces of the eastbound and westbound lanes, respectively; and (c) vertical mixing induced by air flow over the traffic stream and the subsequent transport of heat to (inversion conditions) or away from (lapse conditions) the ground.

To aid this analysis and understanding, the vertical temperature profile data have been examined in more detail. First, the 15-min vertical wind profiles for the near-roadway upwind tower were analyzed to obtain eddy diffusivity values (K, cm^2/s). Because of the relatively few anemometers and the possible influence of traffic and other local surface discontinuities, the eddy diffusivity for momentum (K_m) was estimated from the value of the friction velocity (u^*, cm/s) obtained from the logarithmic wind profile equations,

$$u^* = k \cdot z(\Delta u/\Delta z) \quad (2)$$

and

$$K_m = ku^*z \quad (3)$$

where

k = the Karman constant (0.43),

u = wind speed, and
z = height.

Next, the atmospheric sensible heat flux density [H, $(J/cm^2)/s$] upwind of the roadway was computed:

$$H = -\rho c_p K_h [(\Delta T/\Delta z) + \Gamma] \quad (4)$$

where

ρ = density (g/cm^3),
c_p = the specific heat at constant pressure [(1.00 J/g)/°C], and
Γ = the dry adiabatic lapse rate (9.8° C/km).

The eddy diffusivity for heat (K_h) has been assumed to equal that for momentum.

The significance of the effect of vertical mixing over and downwind of the roadway on the cross-road temperature gradient is clarified by examination of the ambient heat flux data. ΔT values were consistently greater with southerly winds; 72 percent of the south-wind cases occur under stable atmospheric conditions. Thus, on the downwind side, the effect of enhanced vertical mixing over the roadway is to increase temperatures near the surface and, as a result, increase the cross-road temperature gradient. With northerly winds, lapse conditions dominate (84 percent), and the mixing decreases temperatures near the surface downwind of the road and also decreases the ΔT values.

To summarize, the effect of vehicle-induced vertical mixing is to increase the magnitude of the cross-road temperature difference under stable conditions and to decrease the difference under lapse conditions. But this effect only moderates the magnitude of ΔT. The source of heat, however, must be either the vehicles or the roadway pavement. If the latter effect dominates, then warmer temperatures should occur downwind part of the day and cooler temperatures should occur at other times (provided the daily average surface temperature is the same for pavement and soil—a reasonable assumption). This type of diurnal pattern is not observed. To understand the significance of vehicle waste heat emissions, the waste heat flux density averaged over the roadway-median area was computed and evaluated against ambient fluxes.

Waste heat emissions from automobiles have been estimated on the basis of the fuel consumption rate for steady driving. Motor gasoline has an energy equivalent of about 3.46×10^7 J/L; it is assumed that 85 percent of the energy is released as sensible heat. Thus, for cruise speeds below 64 km/h, the waste heat emission rate per vehicle is 3.46×10^6 J/km; above that speed, the heat emission increases at a rate of 2.279×10^4 $(J/km^2)/h$. The resultant heat flux density is then given as the product of the speed-dependent emission rate and vehicle volume divided by the roadway width (36.6 m, including median). The vehicle heat emission rate is generally in the range of 1.4 to 2.1×10^2 W/m^2, with a peak value of 2.5×10^2 W/m^2; for comparison, the peak solar flux density is 5.5×10^2 W/m^2, while the ambient sensible fluxes are generally a factor of five less than the vehicle fluxes.

To further understand the implications of these data, the magnitude of the temperature lapse rates that result from the vehicle heat emissions alone was estimated using Equation 4. The eddy diffusivity above and close to the roadway surface was assumed to be caused primarily by the effect of vehicle motions. Considering K as the product of a turbulent velocity (V*) and a characteristic length scale (ℓ), we let V* equal the vehicle speed and ℓ equal the square root of the vehicle frontal area ($\ell \approx 2$ m). Temperature lapse rates estimated this way are generally in excess of the autoconvective lapse rate. It is unrealistic to exclude the advection of sensible heat from the regions upwind of the roadway. To estimate the combined effects of ambient and vehicular heat fluxes and diffusivities, the arithmetic sum of each was computed to obtain a net vertical temperature gradient from Equation 4. The combined effect is to further enhance instability by day; even for most periods of stable ambient conditions (except when traffic volumes are very low), the vehicle heat emission is sufficient to create an unstable state over the roadway.

These findings are confirmed by the observational data given in Figure 5, where cumulative frequency distributions of the vertical temperature differences (2 to 3.8 m, 3.8 to 7.5 m, and 7.5 to 14.2 m) are given for both the upwind and downwind sides of the road. The decrease in stability downwind of the roadway is apparent at all levels, though most pronounced near the surface.

DISCUSSION

The wind and turbulence data are harder to interpret than either the temperature or tracer gas data. The wind and turbulence data are more influenced by local effects and thus may not provide a true picture of the general flow regime. The apparent dichotomy of the

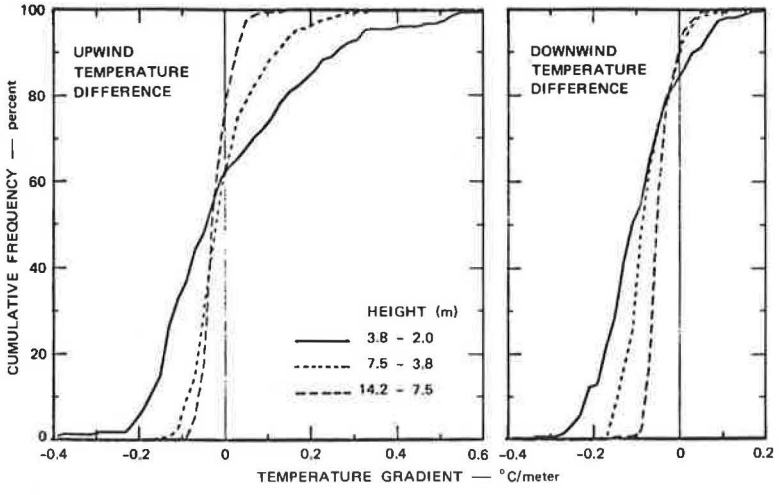

Figure 5. Cumulative frequency distributions of vertical temperature gradients.

turbulence observations is that, although turbulence levels are enhanced significantly by the roadway, they are not correlated with traffic parameters. This suggests that either the turbulence generation mechanism is insensitive to traffic volume and speed variations over the ranges observed or other effects need to be considered; in fact, both concepts may be true.

Further examination of the tracer dispersion data supports the traffic-insensitivity concept. Differences in the dispersion from the upwind and downwind lanes do not correlate significantly with any of the traffic or meteorological parameters tested. Yet the individual dispersion coefficients from both traffic streams correlate well with meteorological parameters alone, as shown in Table 1. But the individual dispersion coefficients do not correlate well with traffic parameters alone and the correlation with the meteorological parameters is not enhanced by the inclusion of traffic volume or vehicle occupancy. Furthermore, the dispersion values correlate negatively with vehicle volume and occupancy alone.

Considering the dispersion of the exhaust gases of a single isolated vehicle, the tailpipe emissions are entrained and rigorously mixed within the wake behind the vehicle. At the same time, the aerodynamic drag of the vehicle imparts a mean flow in the direction of the vehicle movement. Thus, we can hypothesize that the effect of the vehicle motion is primarily to disperse the emissions in a plane oriented vertically and parallel to the roadway. (Some lateral mixing occurs because of the streamline divergence of the flow about the vehicle. The extent of this region is on the order of one obstacle width for fully turbulent atmospheric flow about a stationary bluff body. The net effect for a multilane roadway, however, would appear to be minimal.) The vehicle-induced vertical mixing does affect the concentration. The remaining question is whether the presence of multiple vehicles in longitudinal proximity increases the vertical extent or intensity of the vertical dispersion. Based on the turbulence and tracer-dispersion observations, the implication is that there is not such amplification that is dependent on either vehicle spacing (i.e., volume) or speed. Measurements at this field site failed to indicate any influence of vehicle speed on turbulence and downwind dispersion. The role of such turbulence appears to be largely to mix the air in the vertical space above the pavement. Wind tunnel experiments, however, showed about a 10 percent increase in air pollutant dispersion as vehicle speed increased from 2 to 20 km/h, and about a 7 percent increase as the speed increased from 20 to 80 km/h.

This suggests that while the turbulence generated by a second automobile may further mix the pollutants emitted by a first automobile, the wake of the first automobile may already be thoroughly mixed such that the further mixing has no effect on the concentration; and the turbulence in the wake of the first automobile is normally sufficiently damped so that there is no dynamic interaction with the wake of the following automobile that could lead to an increase in the depth of the mixed zone. However, the mean depth of the mixed zone is a function of vehicle density and speed insofar as these factors affect the thermal instability over the roadway. As vehicles are in disturbed zones of one another, the drag and turbulence intensity per vehicle decrease.

The lateral (i.e., cross-roadway) dispersion is apparently not enhanced by increasing vehicle density or speed. However, consideration of the static effect that a wall of vehicles imparts on the cross-roadway wind and turbulence structure and subsequently on the cross-roadway pollutant dispersion may be necessary. Heretofore this shelterbelt effect has not been considered in understanding near-roadway dispersion. Several studies (1) have been made of the effects of shelterbelt porosity on both the magnitude and extent of the wind speed reduction; Figure 6 illustrates the sheltering at different porosities. The maximum velocity reduction at a single point occurs with a near-solid obstruction, and the maximum sheltering (i.e., spatial integral of velocity deficit) has been observed with porosities of 30 to 50 percent.

The accompanying shear in the mean vertical gradients of velocity enhances the turbulent wind fluctuations and the net transfer of momentum and mass. Plate (2) reports that the intensity of turbulence in the blending region (i.e., the leeward zone where the ambient and disturbed flows merge) increases at a rate proportional to $(u_\infty^2 - u_b^2)(u_\infty - u_b)$, where u_∞ is the ambient cross-shelter wind speed and u_b is wind speed through a porous shelter. Figure 6 shows that the following peak turbulence levels are likely to result:

Shelter Type	Approximate Porosity (%)	Approximate Density (%)	Relative Turbulence Intensity (%)
Solid wall	0	100	100
High density	25	75	83
Medium density	50	50	57
Low density	75	25	53

As an approximation, turbulence levels in the lee of a stationary shelter having an effective porosity typical of that for a heavily traveled roadway may be about one-half those in the lee of a solid wall. For low- to medium-density shelters, turbulence values are relatively insensitive to porosity changes.

These shelterbelt concepts are useful, inasmuch as they provide some insight into the dispersion effects generated by simple, stationary obstructions. The roadway situation is more complex for several reasons, particularly because the drag flow created by traffic motion makes the problem three-dimensional and the relatively simple picture given above may not strictly

Table 1. Matrix of correlation coefficients.

Independent Variables	Dependent Variables: σ Upwind	σ Downwind
σ_w/u_{road}	0.84	0.87
σ_ϕ/u_{road}	0.84	0.90
Traffic volume (Vol)	-0.43	-0.42
Vehicle occupancy	-0.43	-0.40
Vol × σ_ϕ/u_{road}	0.84	0.90
σ_ϕ/vol × u_{road}	0.52	0.48

Figure 6. Sheltering at different porosities.

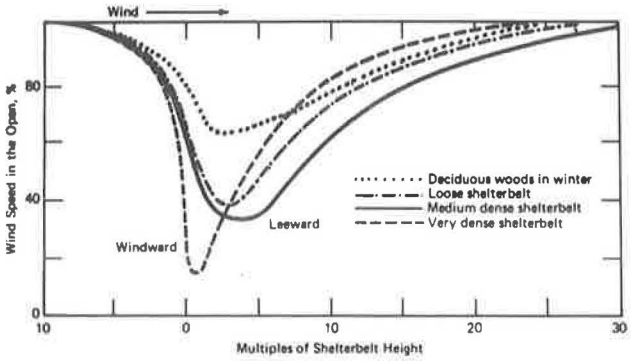

apply. Analysis of these effects is incorporated implicitly into the ROADMAP dispersion methodology, together with the effects introduced by the configuration of the roadway.

ROADMAP

The foundation of the ROADMAP model is the approach used to represent the dispersion of pollutants from an extended line source (end effects are not considered). The model treats the total dispersion as the vector sum of two components: one is the dispersion along the horizontal wind component perpendicular to the roadway, the other is the dispersion along the horizontal wind component parallel to the roadway:

$$\chi_T U/Q_\ell = \vec{i}\ (\chi_n u/Q_\ell) + \vec{j}\ (\chi_p v/Q_\ell) \quad (5)$$

where

$\vec{i}$ = unit vector normal to roadway,
$\vec{j}$ = unit vector parallel to roadway,
U = vector wind speed (m/s),
u = wind component normal to roadway (m/s),
v = wind component parallel to roadway (m/s),
Q_ℓ = line source emission flux density [(g/m)/s],
χ_T = total pollutant concentration (g/m^3),
χ_n = concentration from lateral dispersion (g/m^3), and
χ_p = concentration from longitudinal dispersion (g/m^3).

When Θ is introduced as the angle between the longitudinal axis of the line source and the wind vector, then

$$u = U \sin \Theta \quad (6)$$

and

$$v = U \cos \Theta \quad (7)$$

Substituting Equations 6 and 7 into Equation 5 and squaring both sides,

$$(\chi_T U/Q_\ell)^2 = (\chi_n U \sin \Theta/Q_\ell)^2 + (\chi_p U \cos \Theta/Q_\ell)^2 \quad (8)$$

For convenience, the first right-hand term in Equation 8 is designated the perpendicular term and the second is called the parallel term.

The form of the perpendicular term is specified in analogy to the Gaussian line source equation for a perpendicular wind,

$$\chi_n U/Q_\ell = \sqrt{2/\pi}/k\sigma_z \left(\exp\{-\tfrac{1}{2}[(z + z' - H)/\sigma_z]^2\} + \exp\{-\tfrac{1}{2}[(z + z' + H)/\sigma_z]^2\} \right) \quad (9)$$

where

k = constant ($H = 0$, $k = 2$; $H \neq 0$, $k = 1$),
σ_z = vertical Gaussian dispersion function (m),
z = height above grade level or above roadway (i.e., depressed section) (m),
z' = height offset from plume rise (m), and
H = roadway height above grade level (m).

A unique feature of Equation 9 is the term z', which serves as a height-modifier to represent the possible change in the height of the plume centerline as a function of distance downwind. This offset could result either from the aerodynamic influence (i.e., shelterbelt) of the traffic stream or from the buoyancy effect of vehicular waste heat emissions. In principle, both σ_z and z' may vary both with distance (x) away from the roadway and atmospheric stability, but not with height.

The parallel dispersion term was formulated to represent the general features of the Gaussian point-source equation when the latter is integrated for a wind aligned parallel to a semi-infinite line source (4). The resulting formulation may be thought of as a type of expanding-box model, where the sides and top of the box are given as exponential functions of height (z) and cross-roadway distance (x). The form chosen assumes the same functional dependence on height as the perpendicular term, but a different cross-roadway dispersion representation (f),

$$\chi_p U/Q_\ell = 1/k\sigma_{z\text{-}0} f\left(\exp -\tfrac{1}{2}\{[(z + z' - H)/\sigma_z]^2\} + \exp\{-\tfrac{1}{2}[(z + z' + H)/\sigma_z]^2\} \right) \quad (10)$$

where

$\sigma_z = \sigma_{z\text{-}o} + a_1 x^{b1}$,
$z' = z'_o + a_2 x^{b2}$,
$f = a_3(c_3 + 2x/W)^{b3}$, and
W = roadway width (m).

When the model is applied to both traffic streams, W is defined as the total roadway width (i.e., from shoulder to shoulder). On the other hand, physical separation of the traffic streams or marked dissimilarities in the traffic volumes (and hence emissions) may suggest application of the model separately for each direction. In this case, W would, of course, be redefined accordingly.

Model Evaluation Procedure

A least squares technique was used to estimate the coefficients of the model. Suppose the generalized nonlinear equation is of the form

$$Y + f(X_1, X_2, \ldots, X_K, \beta_1, \beta_2, \ldots, \beta_p) \quad (11)$$

where f is a nonlinear function of k independent variables $X_1, \ldots, X_K$ and p coefficients $\beta_1, \ldots, \beta_p$. We want to choose estimated values of the coefficients such that the sum of squared errors is minimized. If we have T observations on Y, $X_1, \ldots, X_K$, then the sum of squared errors is

$$S = \sum_{t=1}^{T} [Y_t - f(X_{1t}, \ldots, X_{Kt}, \beta_1, \ldots, \beta_p)]^2 \quad (12)$$

To minimize S with respect to the β's, we differentiate the right side of this equation with respect to each coefficient and set the derivatives equal to 0:

$$\sum_{t=1}^{T} 2[Y_t - f(X_{1t}, \ldots, X_{Kt}, \beta_1, \ldots, \beta_p)]\ \partial f/\partial \beta_1 = 0, \text{ for } i = 1, \ldots, p \quad (13)$$

Rather than solving these equations simultaneously, the statistical package for the social sciences (SPSS) program (5) employs the steepest-descent method, an iterative process, to find the minimum value of S. This method moves from one set of coefficient values for $\beta_1, \ldots, \beta_p$ to a new set in such a way that the derivatives (calculated numerically) $-\partial S/\partial \beta_1, \ldots, -\partial S/\partial \beta_p$ are as large as possible, so that those values of $\beta_1, \ldots, \beta_p$ that minimize S are reached rapidly.

Two potential pitfalls exist with this method: (a) the minimum value of S found may be a local rather than a global minimum and (b) the coefficient estimates may not converge at all. Because of the form of the partial

derivatives, it may be impossible to obtain coefficient estimates that represent even a local minimum of the sum of squared errors.

The only measure of the efficiency of the solution provided by the SPSS program (aside from the explained variance) is the number of digits of accuracy (d). Let $\Phi(\beta)$ be the sum of squared errors at the point $\beta = (\beta_1, \ldots, \beta_p)$. A point $\beta^* = (\beta_p^*, \ldots, \beta_p)$ is a d-digit solution if $\Phi(\beta^*) < \Phi(\beta)$ for all β that satisfy: $10^{-d} < \text{rel}_{AX}(\beta^*, \beta) \leq 10^{-d+1}$, where

$$\text{rel}_{AX(\beta^*,\beta)} = \max_{1\leq i\leq p} \{(|\beta_i^* - \beta_i|)/[\max(|\beta_i^*|, |\beta_i|, AX)]\} \quad (14)$$

In the runs of the program to estimate the model, AX was set equal to 0.1 and d equal to 3. When a three-digit solution is impossible because of rounding errors or the nature of the model, the program stops and prints an accuracy estimate with the final coefficients.

In practice, the procedure to evaluate the nine coefficients of the model ($a_1, b_1, \sigma_{z\text{-}o}, a_2, b_2, z_o', a_3, b_3$, and c_3) consists of the following four steps:

1. Step 1—The experimental tests are first stratified according to atmospheric stability. All wind tunnel tests are representative of neutral conditions. The atmospheric tests include stable, neutral, and unstable conditions.
2. Step 2—Coefficients $a_1, b_1, \sigma_{z\text{-}o}, a_2, b_2$, and z_o' are estimated using Equation 9 and those test data with near-orthogonal wind-roadway angles (Θ). For the wind tunnel tests, Θ values $\geq 60°$ are used, and for the atmospheric tests $\Theta \geq 63°$. The variance (R^2) explained by the estimated coefficients and Equation 9 are also determined for the large-Θ cases.
3. Step 3—Next, coefficients a_3, b_3, and c_3 are estimated using Equation 10, the other coefficient estimates from Step 2, and those test data with near-parallel wind-roadway angles. For the wind tunnel tests, Θ-values $\leq 15°$ are used; for the atmospheric tests $\Theta \leq 24°$. Again, R^2 is determined.
4. Step 4—Equations 9 and 10 are substituted into the general model form, Equation 8, together with the nine coefficient estimates from steps 2 and 3. In this way, the component ROADMAP model is used to predict normal concentrations for all observed data. Observations and predictions are then compared for all data, as well as for various subsets including those cases not included in the coefficient estimates of steps 2 and 3; the latter provide an independent test of ROADMAP performance.

Model Performance

Step 4 of the model evaluation procedure provides the basis for an independent test of ROADMAP. In this step, the dispersion coefficients estimated from the near-parallel and near-perpendicular wind direction cases are used in the model to predict normal concentrations at each of the downwind sampling locations. This procedure is applied to all wind tunnel and atmospheric tests. The stability for all wind tunnel tests is neutral, whereas the atmospheric data include diabatic conditions as well.

Three meteorological parameters measured upwind of the roadway are used to classify stability for the grade-level test data; unfortunately, none of the three is consistently successful by itself and it is necessary to consider the three jointly. The three parameters used included: (a) standard deviation of the horizontal wind direction (σ_Θ), (b) standard deviation of the vertical wind direction (σ_ϕ), and (c) gradient Richardson number (Ri). As only 45 h of data were available at the grade-level site, it was necessary to stratify the data into three broad stability classes, simply referred to as unstable, neutral, and stable. Tabulated below are the ranges of each parameter for each stability class:

Class	Number of Hours	$\sigma(e)$ (degrees)	$\sigma(\phi)$ (degrees)	Ri, n.d.
Unstable	9	16.8 to 40.9	7.4 to 22.2	-4.61 to -0.03
Neutral	17	5.6 to 15.6	2.9 to 12.5	-0.83 to 0.37
Stable	7	17.1 to 47.9	4.4 to 24.0	0.00 to 0.12

In addition to using these three parameters in an objective way, qualitative use was made of the temperature lapse rate, time of day, and cloud cover in assigning the hourly periods to the three stability classes. Even so, 12 h did not fit even these loose criteria and were not included in the analysis.

Before testing the model's performance, two aspects of the stability categorization should be stressed, particularly as stability is an important determinant of the dispersion process. First, the values of σ_Θ for stable conditions are very large, ranging from 17° to 48°. Much larger, for example, than the usual range of 5° to 10° reported in the air pollution literature (6). Note, however, that the accompanying wind speeds were very light (in the range of 1-3 m/s) and that a slow meander of the wind direction is common under these conditions. Second, the large magnitude of these horizontal wind fluctuations has no appreciable effect on dispersion from an extended line source with an oblique wind direction. But when the wind is near-parallel to the roadway, the effect is to significantly enhance the lateral dispersion and reduce the pollutant concentrations well below what would be estimated using the standard range of σ_Θ. This is a particularly significant aspect of line-source dispersion and the accurate assessment of σ_Θ is critical for wind directions with a significant component parallel to the roadway.

The results of the ROADMAP evaluation are summarized in Table 2 for each of seven cases of atmo-

Table 2. Summary of ROADMAP evaluation with independent data from atmospheric and wind tunnel experiments.

Test Description	θ-Range (degrees)	Number of Data Periods	Number of Data Points	Statistics r	r^2	m	s
Atmospheric tests							
Grade-level, neutral stability	19 to 62	6	90	0.908	0.824	0.084	1.06
Grade-level, stable atmosphere	≤68	5	75	0.666	0.444	0.000	0.51
Grade-level, unstable atmosphere	25 to 66	5	75	0.803	0.645	0.035	0.71
Wind tunnel tests							
Vertical-wall cut	30	4	60	0.692	0.479	0.076	0.71
Slant-wall cut	30	4	60	0.836	0.699	0.054	0.50
Fill section	30	4	60	0.934	0.873	-0.011	2.42
Viaduct section	30	4	60	0.917	0.841	-0.010	2.57

Notes: r = linear correlation coefficient.
r^2 = fractional variance explained.
m = regression intercept (m^{-1}), s = slope of linear regression } $\left(\frac{\chi u}{Q}\right) = m + s\left(\frac{\chi u}{Q}\right)_{calc}$

spheric stability and roadway configuration. The results are very encouraging, although it would be both informative and constructive to test the model with a larger data set as well as with data from other, similar sites.

Dispersion Patterns

The derived dispersion coefficients (σ_z, z′, and $f\sigma_{z\text{-}o}$) and the model provide an effective means for synthesizing ing the dispersion characteristics of the test data and for obtaining a generic picture of the overall dispersion pattern. Figure 7 shows the variation of the three dispersion coefficients with distance from the roadway. These curves were derived from the CO concentration data; as the evaluation process does not consider variations in CO emission rates among the six lanes (or two directions either), it is not appropriate to attach significance to those portions of the curves that extend over the roadway surface. Perhaps most significant is the sign and magnitude of the z′ term. The nearly constant and negative value indicates that the centerline of the exhaust plume is found about 1.5 m above ground downwind of the roadway. This lifting of the plume may reflect the impact of either the waste-heat or shelterbelt effects discussed earlier.

Figure 7. ROADMAP dispersion parameters—grade-level roadway, smooth terrain, and neutral atmospheric conditions.

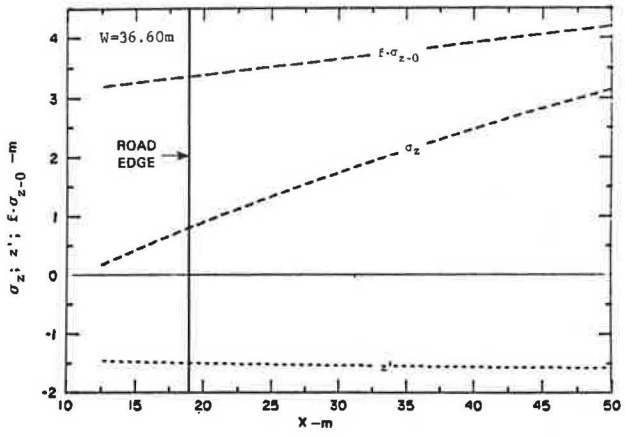

The dispersion coefficients illustrated in Figure 7 have been used as input to ROADMAP to construct isopleths of normal pollutant concentrations for joint variations in the wind-roadway angle (Θ) and road-receptor separation (x). Figure 8 is such a contour plot and is appropriate to neutral atmospheric stability and a 1-m receptor height. A noteworthy feature of the plot is the lack of a strong dependence of X_u/Q on Θ; as discussed earlier, this reflects the significant lateral diffusion that can occur as a result of wind meander, which thereby retards the increase in concentration levels when the wind direction becomes nearly parallel to the roadway. The contours obtained from computations made with the U.S. Environmental Protection Agency (EPA) HIWAY model are in contrast to this moderate Θ-dependence (see Figure 9). Not only is there a strong concentration gradient, but the HIWAY model also predicts significantly larger concentration levels than does ROADMAP. The difference between the two models can be explained by the height-offset term (z′), which is not a feature of other line-source models, such as HIWAY (1), as well as the large lateral dispersion values used in ROADMAP. When the HIWAY model was evaluated against the US-101 data, it consistently overpredicted (3) concentrations when the cross-roadway wind component was less than 1.5 m/s. We, therefore, conclude that the current

Figure 8. ROADMAP values of normal concentrations near ground level for at-grade roadway, smooth terrain, and neutral atmospheric stability.

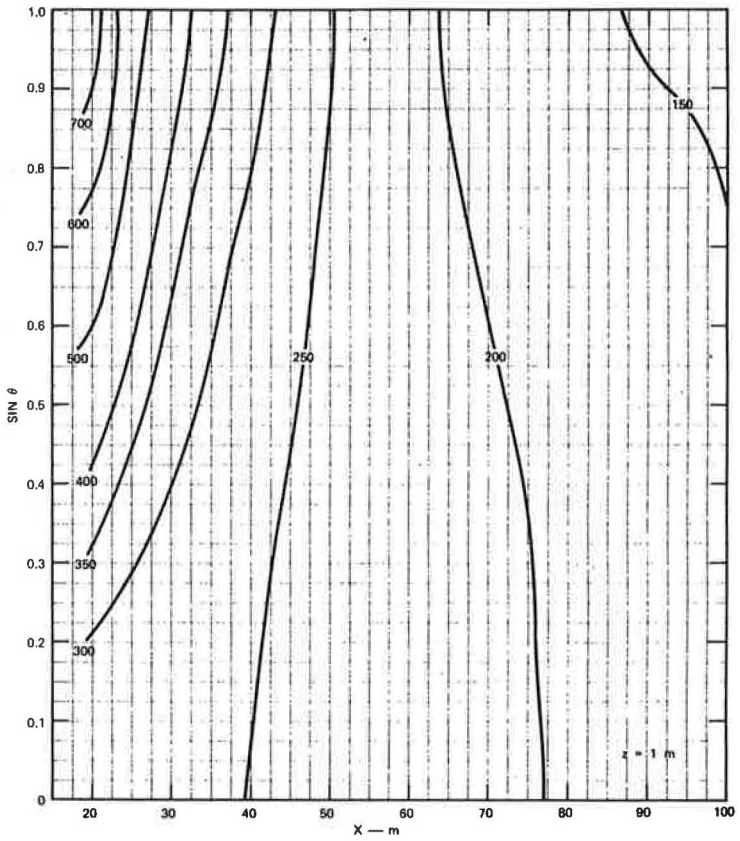

Figure 9. HIWAY values of normal concentrations near ground level for at-grade roadway, smooth terrain, and neutral atmospheric stability.

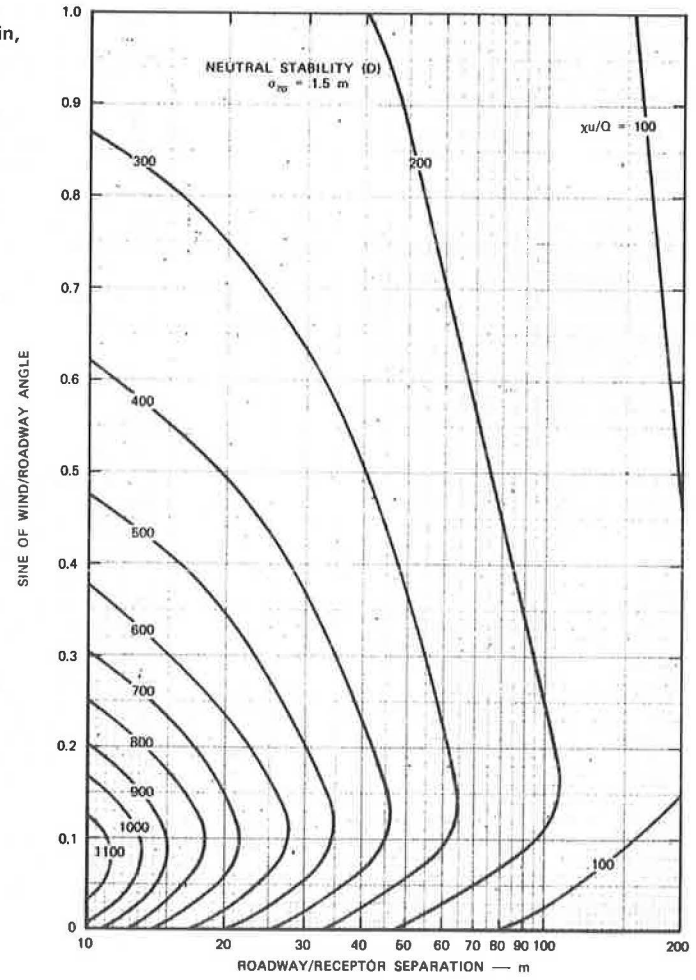

Figure 10. ROADMAP values of normal concentrations at three heights for at-grade roadway, smooth terrain, and neutral atmospheric stability.

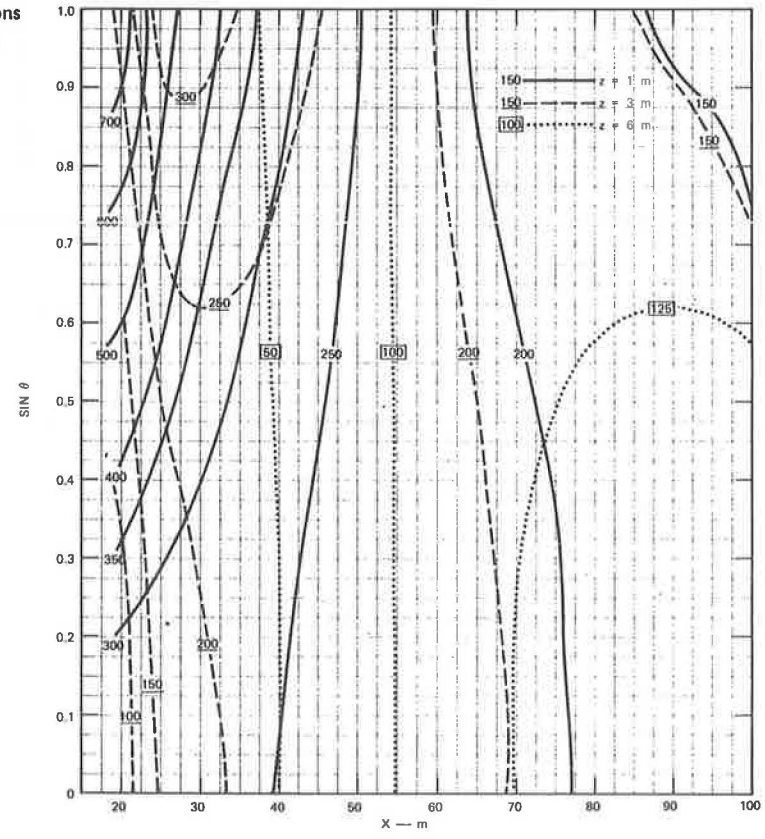

body of data both indicates a better performance by ROADMAP, and implicitly supports the value of the concepts incorporated within the height-offset and lateral diffusion terms.

Applying ROADMAP to greater heights, we generate the composite contour plot seen in Figure 10. Using three different line types, the figure illustrates the isopleths of normal concentration at heights of 1, 3, and 6 m.

Wind Tunnel Data

Before exploring the implications of the wind tunnel tests, we first examine the representativeness of the data. That is, a comparison of the dispersion patterns obtained from the atmospheric study of US-101 with data from a comparable configuration in the wind tunnel is desirable. This scale model test was not intended to duplicate precisely the atmospheric test, and as such a few discrepancies are noted:

1. The scale model has four traffic lanes to six for the atmospheric site;
2. There is no azimuthal meander of the wind direction in the wind tunnel; and
3. The uniformity of the traffic speed, volume, and emissions is in distinct contrast to the atmospheric test conditions.

Figure 11 illustrates the variation of the three dispersion coefficients in the wind tunnel. The σ_z and z′ terms are quite similar in shape and magnitude to the atmospheric equivalents shown earlier in Figure 7. In contrast, the lateral term ($f\sigma_{z\text{-}o}$) is markedly different: near the roadway edge it is very small, indicating high concentrations, but further away it increases rapidly, indicating a corresponding drop in concentration. This is consistent with the steady-wind concept (i.e., no meander). In the atmospheric test, $f\sigma_{z\text{-}o}$ is nearly independent of x, indicating a more uniform horizontal X-distribution with parallel winds—typical of the meander concept.

The dispersion coefficients shown in Figures 7 and 11 are then used in ROADMAP to compute concentration values to compare objectively the dispersion patterns at 16 common receptor locations (see Figure 12). Comparisons were made over a 4 × 4-receptor matrix with z = 1, 2, 4, and 8 m and x = 20, 30, 40, and 50 m; two wind-roadway angles were considered: Θ = 0° and 90°. Considering first the parallel wind situation, the atmospheric data yield an average Xu/Q of 0.14/m and the wind tunnel average is 0.124/m. Moreover, the higher-concentration receptors (i.e., small x and z) indicate wind tunnel concentrations about 60 percent greater than their atmospheric counterparts, but further away from the roadway the atmospheric values drop off very little in comparison to the wind tunnel concentrations, which rapidly approach zero. The low correlation value of 0.44 reflects this convolution. Referring to the oblique wind data, the average concentration is nearly two-thirds greater for the atmospheric data and the value of the linear correlation coefficient increases to a very significant 0.87. From these comparisons we conclude that the relative dispersion pattern given by the wind tunnel data is representative of atmospheric conditions when the wind-roadway angle has a strong oblique component, but the lateral dispersion is underestimated in the wind tunnel for near-parallel wind-roadway angles.

Configuration and Stability Effects

Figures 13 to 18 illustrate the x-dependence of the three dispersion coefficients for various roadway configurations and atmospheric stability conditions. Figures 13 and 14 represent the unstable and stable cases for the atmospheric, grade-level roadway experiment. Figures 15 through 18 are from the wind tunnel tests of four roadway configurations: vertical-wall cut, slant-wall cut, fill section, and viaduct section.

CONCLUDING REMARKS

A comprehensive series of atmospheric and wind tunnel aerometric experiments has provided new insights into the effects of vehicular traffic, meteorology, and roadway configuration on the microscale dispersion of vehicular emissions. When the roadway configuration is simple (i.e., smooth, grade-level configuration), two traffic-induced effects are important: (a) vehicular waste heat emissions and (b) the aerodynamic obstruction that the traffic stream presents to the wind flow. To account for these effects and those imparted by the roadway geometry, a new and simple empirical model called ROADMAP has been developed and evaluated. The model's performance and versatility have been shown to be quite encouraging; evaluations against independent data show correlation coefficients that range from 0.67 to 0.93 for a wide range of stability conditions and roadway configurations.

Figure 11. ROADMAP dispersion parameters—grade-level roadway and smooth terrain (wind tunnel test).

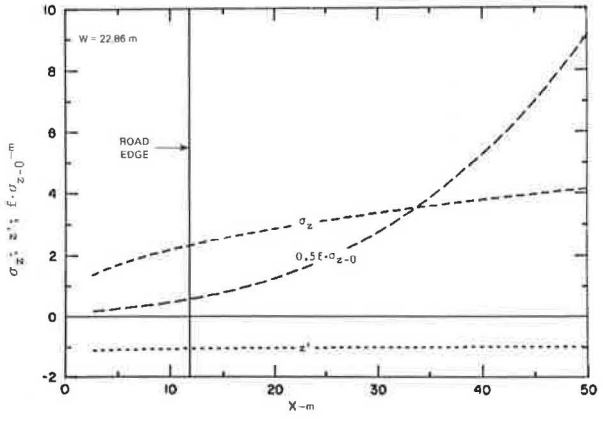

Figure 12. ROADMAP values of normal concentrations from comparable atmospheric and wind-tunnel analyses, neutral stability, and grade-level roadway.

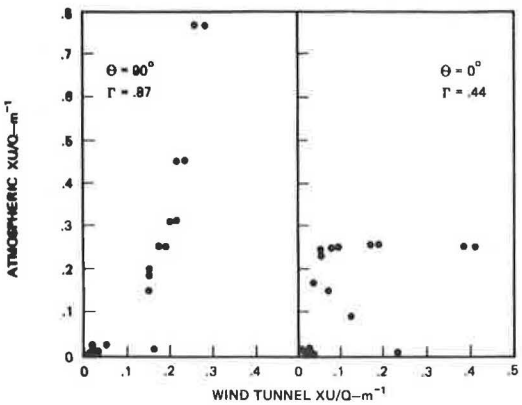

ACKNOWLEDGMENTS

The research reported in this paper was supported by the Office of Research, Federal Highway Administration. The logistical support of the California Department of Transportation and EPA during the atmospheric tests is gratefully acknowledged. In addition, the invaluable and willing assistance of a number of Stanford Research Institute colleagues is greatly appreciated and acknowledged: C. Flohr, D. Marimont, R. Pozdena, R. Ruff, L. Salas, E. Shelar, and A. Smith. The wind-tunnel measurements were made by G. Ludwig and G. Skinner under a subcontract with Calspan Corporation, Buffalo, New York.

Figure 13. ROADMAP dispersion parameters—grade-level roadway, smooth terrain, and unstable atmospheric conditions.

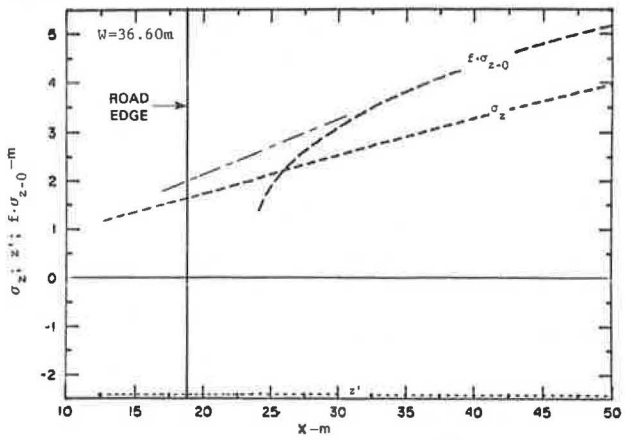

Figure 14. ROADMAP dispersion parameters—grade-level roadway, smooth terrain, and stable atmospheric conditions.

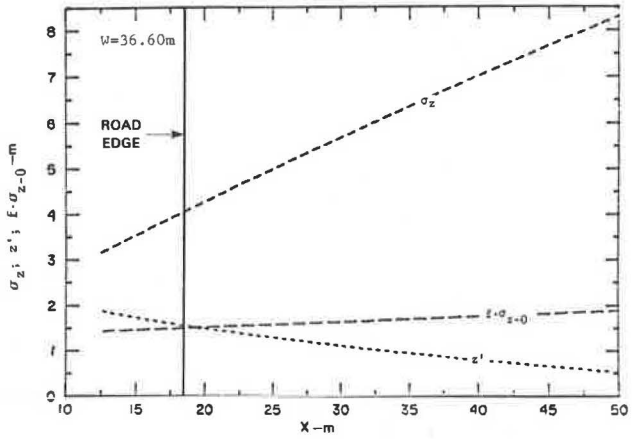

Figure 15. ROADMAP dispersion parameters—cut section with vertical walls and smooth terrain (wind tunnel test).

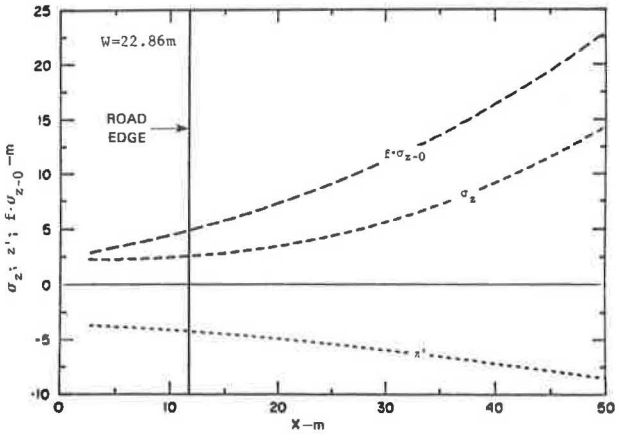

Figure 16. ROADMAP dispersion parameters—cut section with sloping walls and smooth terrain (wind tunnel test).

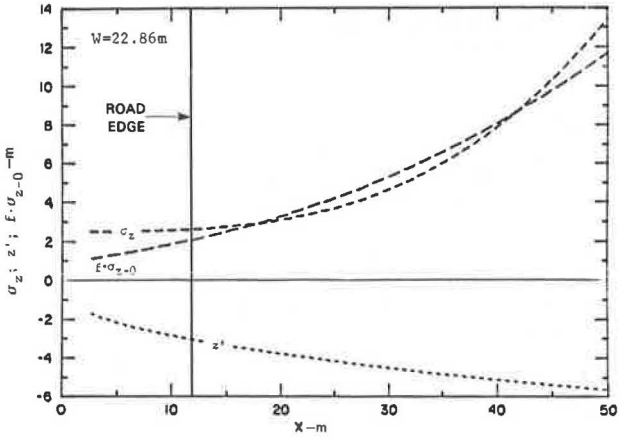

Figure 17. ROADMAP dispersion parameters—fill section and smooth terrain (wind tunnel test).

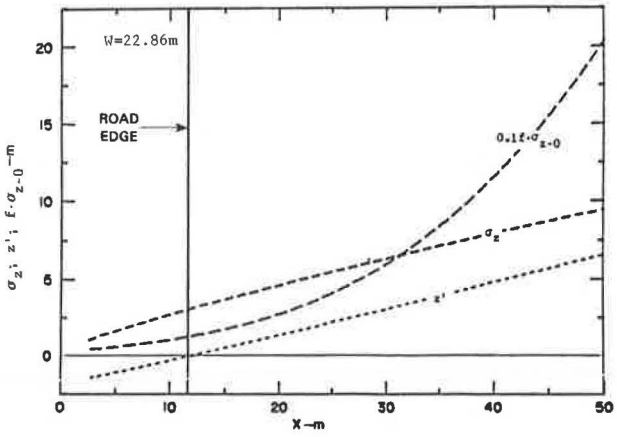

Figure 18. ROADMAP dispersion parameters—viaduct section and smooth terrain (wind tunnel test).

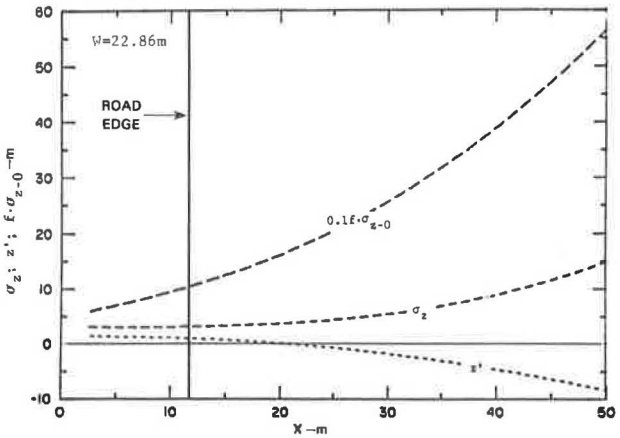

REFERENCES

1. W. Nageli. Untersuchungen uber die Windverhaltnisse in Bereich von Windschutzstreifen. Mitt. Schweiz. Anst. Versuchsw., Vol. 23, 1941, pp. 221-276.
2. E. J. Plate. Aerodynamic Characteristics of Atmospheric Boundary Layers. Atomic Energy Commission Critical Review Series, TID-25465, 1971.
3. W. F. Dabberdt and others. Rationale and Evaluation of Guidelines for the Review of Indirect Sources. Stanford Research Institute International, Menlo Park, CA, Final Rept. Proj. 4429, 1976.
4. W. F. Dabberdt and R. C. Sandys. Guidelines for the Review of Indirect Sources. Stanford Research Institute International, Menlo Park, CA, Final Rept. Proj. 4429, 1976.
5. N. H. Nie and others. Statistical Package for the Social Sciences. McGraw-Hill, New York, 1975.
6. F. L. Ludwig and W. F. Dabberdt. Comparison of Two Practical Atmospheric Stability Classification Schemes in an Urban Application. Journal of Applied Meteorology, Vol. 15, No. 11, 1976, pp. 1172-1176.
7. J. R. Zimmerman and R. S. Thompson. User's Guide for HIWAY, a Highway Air Pollution Model. U.S. Environmental Protection Agency, Research Triangle Park, NC, EPA-650/4-74-008, 1975.

Overview of the New York State Long Island Expressway Dispersion Experiment

S. Trivikrama Rao, Marsden Chen, Michael T. Kennan, Gopal Sistla, Perry J. Samson, and David Romano, Division of Air Resources, New York State Department of Environmental Conservation

The objective of this investigation was to collect particulate, gaseous, micrometeorological, and traffic data adjacent to a major highway in a nonurban setting. The experimental site was on a section of the Long Island Expressway that is heavily traveled and where development adjacent to the roadway is relatively minor. The data base is useful for (a) documentation of the distribution of sulfate, lead, total particulate, and carbon monoxide levels at an array of sampling points near the highway; (b) study of the micrometeorological structure adjacent to the highway with special attention to those parameters that are important in the determination of sigma and stability values as well as highway-generated turbulence; (c) reevaluation of highway air pollutant emission factors from the data gathered on tracer gas experiments; and (d) validation of several highway dispersion models. The location of the site and data acquisition techniques are presented. The experimental design of the roadway diffusion study is described and some of the preliminary results of the tracer gas release experiments and sulfate and lead measurements are presented. The data collected in this investigation are being analyzed and a more comprehensive analysis will be presented elsewhere.

Mathematical modeling techniques are being employed to estimate the pollutant concentrations adjacent to highways. A number of mathematical models have been developed for the prediction of pollutant levels, but only a few experimental programs have been undertaken for establishing a sufficiently detailed data base (consisting of traffic, pollutant concentrations, and meteorological data) to be used for model verification. In recent years, such studies were conducted by Stanford Research Institute, General Motors Corporation, and New York State Department of Environmental Conservation. The General Motors study was a controlled experiment on a test track, whereas the Stanford Research Institute and New York State studies were carried out along major highways.

EXPERIMENTAL PROCEDURES

The site chosen on the Long Island Expressway (I-495) is about 25 km east of the city limits of New York City. Figure 1 is a map of the sampling area, which shows nearby residential areas and highways. Recent estimates of vehicles per day as reported by the Suffolk County Highway Department are indicated next to the highways. The area does not contain any major industrial centers; the nearest large point sources are 6 km to the southwest in Bethpage. The highway at the site is fairly flat and straight. The land to the north and the south of the site is a sod farm and is undeveloped and open. Because of the relatively undeveloped nature of the location, the high vehicle density, the flatness of the terrain, and the distance from other highways and point sources, this site closely approximates the assumptions common to all at-grade dispersion models.

Data Collection and Equipment

A network of towers and sensors was designed and adapted for the project in order to collect data, both upwind and downwind, in a vertical plane perpendicular to the highway. Figure 2 shows the layout of these towers (looking west) and the specific location of air quality and meteorological measurements. A 12-m trailer that housed the instrumentation needed for this study was located about 100 m from the edge of the road and 20 m to the west of the sampling grid on the south side of the highway. This distance was necessary for minimal interference with the wind flow characteristics at the sampling plane. The trailer housed the data acquisition sys-